STE20-Type Kinases MST3 and MST4 Act Non-Redundantly to Promote the Progression of Hepatocellular Carcinoma

Mara Caputo
University of Gothenburg and Sahlgrenska University Hospital
Ying Xia
University of Gothenburg and Sahlgrenska University Hospital
Sumit Kumar Anand
University of Gothenburg and Sahlgrenska University Hospital
Emmelie Cansby
University of Gothenburg and Sahlgrenska University Hospital
Emma Andersson
University of Gothenburg and Sahlgrenska University Hospital
Hanns-Ulrich Marschall
University of Gothenburg and Sahlgrenska University Hospital
Alfred Königsrainer
University Hospital Tübingen
Andreas Peter
University Hospital Tübingen
Margit Mahlapuu (margit.mahlapuu@gu.se)
University of Gothenburg and Sahlgrenska University Hospital

Research Article

Keywords: MST3, MST4, STE20-type kinases, non-alcoholic steatohepatitis, hepatocellular carcinoma, hepatocellular lipid droplets

Posted Date: February 17th, 2023

DOI: https://doi.org/10.21203/rs.3.rs-2586984/v1

Abstract

Aims

Hepatocellular carcinoma (HCC) is one of the most fatal and fastest-growing malignancies. Recently, non-alcoholic steatohepatitis (NASH), characterized by liver steatosis, inflammation, cell injury (hepatocyte ballooning), and different stages of fibrosis, has emerged as a major catalyst for HCC. Because the STE20-type kinases MST3 and MST4 have been described as critical molecular regulators of NASH pathophysiology, we here focused on determining the relevance of these proteins in human HCC.

Methods

The clinical importance of MST3 and MST4 in HCC was assessed in publicly available datasets and by qRT-PCR analysis of a validation cohort recruited at the University Hospital of Tübingen (n = 48 for HCC patients and n = 214 for control subjects). The functional significance of MST3 and MST4 was examined in HepG2 and Hep3B cells transfected with *MST3*, *MST4*, or *MST3/4* small interfering RNA. Potential downstream pathways were investigated by co-immunoprecipitation and Western blotting.

Results

By analyzing public datasets and in-house cohorts, we found that hepatic *MST3* and *MST4* expression was positively correlated with the incidence and severity of HCC. We also found that the silencing of both MST3 and MST4, but also either of them individually, markedly suppressed the tumorigenesis of human HCC cells including attenuated proliferation, migration, invasion, and epithelial-mesenchymal transition. Mechanistic investigations revealed lower activation of STAT3 signaling in MST3/MST4-deficient hepatocytes, and identified GOLGA2 and STRIPAK complex as the binding partners of both MST3 and MST4 in HCC cells.

Conclusions

These findings reveal that MST3 and MST4 play a critical role in promoting the progression of HCC and suggest that targeting these kinases may provide a novel strategy for the treatment of liver cancer.

Introduction

Hepatocellular carcinoma (HCC) is the 3rd most common malignancy in terms of cancer-related mortality, causing more than 830,000 deaths globally each year (1, 2). The efficacy of current anti-HCC therapies is not satisfactory, and most HCC patients develop disease progression with a low 5-year survival rate of 18% and a high recurrence rate of 70% (1, 3). Well-known etiologic factors for HCC are hepatitis B and C virus infection and chronic alcohol consumption (1, 4). Recently, there has been a rapid increase in the

proportion of HCC attributed to non-alcoholic steatohepatitis (NASH), which is expected to become the most common cause of HCC in the near future (5–7). As the precursor step in the development of HCC in patients with obesity or diabetes mellitus, NASH is characterized by hepatic steatosis as well as liver inflammation, cell injury (hepatocyte ballooning), and different stages of fibrosis (8, 9). Despite the high medical need, the pathophysiological mechanisms underlying the initiation of NASH, and the aggravation of NASH into HCC, remain poorly characterized. Hence, understanding the molecular causes for the development of NASH, and for switching from NASH to HCC, represents a major challenge necessary to accelerate the discovery of novel targeted therapies.

Our recent translational studies have identified the STE20-type kinases MST3 (Mammalian Sterile 20-Like 3; also known as STK24) and MST4 (Mammalian Sterile 20-Like 4; also known as STK26 or MASK) as critical molecular regulators of NASH pathophysiology. We found that *MST3* and *MST4* mRNA levels in human liver biopsies are positively correlated with the clinical features of NASH (*i.e.*, hepatic steatosis, lobular inflammation, and hepatocellular ballooning)(10, 11). Furthermore, we observed that the silencing of MST3 or MST4 in cultured human hepatocytes blocks intracellular lipid accumulation by enhancing mitochondrial β-oxidation and triacylglycerol (TAG) efflux while reducing fatty acid uptake and lipid synthesis (10, 11). Reciprocally, a marked increase in intracellular fat storage was detected in human hepatocytes overexpressing MST3 or MST4 (10, 11). We also found that systemic administration of *Mst3*-targeting antisense oligonucleotides in mice substantially suppresses the full spectrum of high-fat diet-induced NASH including liver steatosis, local inflammation, and fibrosis (12). Of note, our studies reveal that MST3 and MST4 proteins are predominantly associated with intracellular lipid droplets in human and rodent hepatocytes (10, 11), which is well-aligned with the emerging view of intrahepatocellular lipid droplets as dynamic organelles that govern lipid partitioning and metabolic dysfunction in the liver (13, 14).

To date, the potential role of MST3 in the development of HCC has not been explored; however, several studies have investigated the involvement of MST4 in HCC. Elevated hepatic MST4 expression has been described as an adverse prognostic factor for survival and recurrence time in patients with HCC (15). In the same study, the depletion of MST4 was demonstrated to inhibit HCC cell proliferation and invasion *in vitro*, whereas the overexpression of MST4 was shown to promote these processes (15). Conversely, a low MST4 abundance has also been reported to associate with the progression of HCC and poor patient prognosis, and the functional inactivation of MST4 was found to increase proliferation, motility, and invasion of human HCC cells *in vitro* and to facilitate intrahepatic metastatic potential *in vivo* (16, 17). Notably, MST3 and MST4 have previously been described to control tumorigenesis in gastric, pancreatic, colorectal, prostate, and breast cancer as well as glioblastoma (18–26). MST3 and MST4 are also implicated in the pathology of endothelial malformations (27–29), in the regulation of neuronal function (30–32), and in immune responses (27, 33, 34).

In this study, we focused on determining the relevance of STE20 kinases MST3 and MST4 in human HCC, and on investigating the possible synergies between these two proteins. Our results demonstrate that the silencing of both MST3 and MST4, but also either of them individually, markedly suppressed the

tumorigenesis of human hepatoma-derived cells. Consistently, we found that *MST3* and *MST4* were up-regulated in human HCC tissues. Together, our data provide the first evidence that MST3/MST4 may serve as potential therapeutic targets for HCC.

Materials And Methods

Liver Samples and Clinical Data

For the analysis of liver tissue samples, a cohort of 262 Caucasian individuals (men, n = 157; women, n = 105) undergoing liver surgery at the Department of General, Visceral, and Transplant Surgery at the University Hospital of Tübingen (Tübingen, Germany) were recruited. The subjects tested negative for viral hepatitis and had no liver cirrhosis.

After food withdrawal overnight, liver samples were taken from normal, non-diseased tissue determined by the pathologist during surgery, immediately snap frozen in liquid nitrogen, and stored at − 80°C. To determine the liver fat content, the samples were homogenized in PBS containing 1% Triton X-100 with a TissueLyser (Qiagen, Hilden, Germany). The concentration of TAG in the homogenate was then quantified using an ADVIA XPT Clinical Chemistry Analyzer (Siemens Healthineers, Eschborn, Germany) and the results were calculated as mg/100 mg tissue weight (%). Quantitative real-time PCR (qRT-PCR) was performed on liver samples as described below using the primers as listed in Supplementary Table S1.

All investigations were performed with approval by the Ethics Committee of the University of Tübingen, Germany (368/2012BO2) and carried out in accordance with the Declaration of Helsinki. Written informed consent was obtained from all patients enrolled in this study.

Data Collection from Public Databases

The whole transcriptome sequencing (RNA-seq) data was downloaded from the Hepatocellular Carcinoma Project in the Cancer Genome Atlas (TCGA) (35) and the Genotype-Tissue Expression Portal (GTEx) (36). We also downloaded two HCC datasets (GSE14520 and GSE36376) from the GEO database. TCGA, GTEx, and GEO databases are publicly available and written informed consent was obtained from the patients prior to data collection.

Cell Culture and Transfection Assays

HepG2 and Hep3B cells (human liver cancer cell lines; American Type Culture Collection, Manassas, VA) were cultured in Dulbecco's Modified Eagle's Medium (DMEM; GlutaMAX supplemented; Gibco, Paisley, UK) supplemented with 10% (vol/vol) FBS and 1% (vol/vol) penicillin/streptomycin (Gibco). Cells were demonstrated to be free of mycoplasma infection by MycoAlert Mycoplasma Detection Kit (Lonza, Basel, Switzerland). Cells were transfected with *MST3* small interfering (si)RNA (139160; Ambion, Austin, TX), *MST4* siRNA (HS01_00030410; Sigma-Aldrich, St. Louis, MO), or scrambled siRNA (SIC001; Sigma-Aldrich) using Lipofectamine RNAiMax (Thermo Fisher Scientific, Waltham, MA). After transfection, cells

were treated with 100 µmol/l oleic acid (Sigma-Aldrich) for 48 h to induce steatosis (Supplementary Figure S1).

Colony Formation and Cell Proliferation Assays

In the colony formation assay, cells were seeded in 12-well plates (1×10^3 cells/well) and cultured for 6 days. Subsequently, colonies were fixed with 4% (vol/vol) of phosphate buffered formaldehyde (Histolab Products, Gothenburg, Sweden), stained with 0.1% crystal violet (Sigma-Aldrich), and counted under the Eclipse TS100 microscope (×10; Nikon, Minato, Tokyo). The proliferation assay was performed using the Click-It EdU Cell Proliferation Kit (Thermo Fisher Scientific) according to the manufacturer's recommendations. Immunofluorescence images were acquired using a Zeiss Axio Observer microscope with the ZEN Blue software (Zeiss, Oberkochen, Germany). The labeled area was quantified in 6 randomly selected microscopic fields (×20) per well using the ImageJ software [1.47v; National Institutes of Health (NIH), Bethesda, MD].

Transwell and Scratch Assays

To assess migration, cells were seeded in the upper chambers of the transwells with 8 µm pore size (Polycarbonate Cell Culture Inserts in Multi-Well Plates; Costar, Kennebunk, ME) and DMEM with 10% FBS was added in the bottom chambers for a chemotactic gradient. In the following day, cells on the top side of the membranes were removed with cotton swabs, and cells on the bottom side were fixed and stained with 0.1% crystal violet. To assess invasion, the transwells were coated with Matrigel matrix (Corning, Bedford, MA) before the experiment. Images were acquired using a Zeiss Axio Observer microscope with the ZEN Blue software as described above and the crystal violet-labeled area was quantified in 6 randomly selected microscopic fields (×20) per well of the cell culture chamber using the ImageJ software.

In the scratch assay, cells were seeded in 6-well plates and a sterile pipette tip was used to make a scratch in the center of the well. The width of the gap was then photographed and measured 0, 24, and 48 h later.

Cell Viability and Apoptosis Analyses

Cell viability was analyzed using the CellTiter-Blue Cell Viability Assay (Promega, Stockholm, Sweden) according to the manufacturer's instructions. The Cell Meter Phosphatidylserine Apoptosis Assay Kit (AAT Bioquest, Pleasanton, CA) was used to detect the initial and intermediate stages of apoptosis by Apopxin Violet labeling.

Immunofluorescence Staining

Cells were fixed in 4% (vol/vol) phosphate buffered formaldehyde and then processed for immunofluorescence with anti-α-fetoprotein (AFP), anti-cytokeratin-19 (CK19), anti-cleaved caspase (CASP)3, anti-E-cadherin, anti-epithelial cell adhesion molecule (EpCAM), anti-fibronectin, anti-glucose regulatory protein 78 (GRP78), anti-Ki67, anti-N-cadherin, anti-proliferating cell nuclear antigen (PCNA), or

anti-YES-associated protein (YAP) antibodies (see Supplementary Table S2 for antibody information). Immunofluorescence images were acquired using a Zeiss Axio Observer microscope with the ZEN Blue software as described above and labeled area was quantified in 6 randomly selected microscopic fields (×20) per well using the ImageJ software.

qRT-PCR and Western Blot

RNA was isolated from liver tissue samples and cultured human hepatocytes with the RNeasy Tissue Kit (Qiagen) or the EZNA Total RNA Kit (Omega Bio-Tek, Norcross, GA), respectively, according to the manufacturer's recommendations. cDNA synthesis was performed using the High-Capacity cDNA Reverse Transcription Kit (Thermo Fisher Scientific). Relative quantification was performed with the LightCycler480 (Roche Diagnostics, Mannheim, Germany) or the CFX Connect Real-Time System (Bio-Rad, Hercules, CA). Relative quantities of target transcripts were calculated from duplicate samples after normalization of the data to the endogenous controls, *RSP13* (TIB Molbiol Syntheselabor GmbH, Berlin, Germany) for human liver tissue or 18S rRNA (Thermo Fisher Scientific) for cultured human hepatocytes. Western blot analysis was performed as previously reported (37) (see Supplementary Table S2 for antibody information).

Immunoprecipitation and Mass Spectrometry

HepG2 cells were transfected with human expression plasmid encoding *MYC-MST3* (EX-T8396-M43; GeneCopoeia, Nivelles, Belgium) or *MYC-MST4* (EX-W0097-M43; GeneCopoeia), or an empty control plasmid (EX-NEG-M43; GeneCopoeia) using Lipofectamine 2000 (Thermo Fisher Scientific). 72 h after transfections, cells were suspended in lysis buffer (50 mmol/l HEPES, 90 mmol/l KCl, 0.5% IGEPAL, and protease inhibitors) and immunoprecipitated with anti-MYC antibodies according to the manufacturer's instructions (Anti-c-MYC Magnetic Beads; Thermo Fisher Scientific). Proteins were eluted from the beads using 200 mmol/l glycine.

The eluted proteins were digested with trypsin and processed using the modified filter-aided sample preparation (FASP) method (38). Briefly, samples were reduced with 100 mmol/l DL-dithiothreitol (DDT) at 37°C for 60 min, transferred to 30 kDa MWCO Pall Nanosep Centrifugation Filters (Sigma-Aldrich), washed repeatedly with 8 mol/l urea and once with digestion buffer [0.5% sodium deoxycholate (SDC) in 50 mmol/l triethylammonium bicarbonate (TEAB)] prior to alkylation with 10 mmol/l methyl methanethiosulfonate for 30 min. The samples were further digested with Pierce MS Grade Trypsin (300 ng; Thermo Fisher Scientific) at 37°C overnight and an additional portion of trypsin was added and incubated for another 3 h. Peptides were collected by centrifugation and SDC was removed by acidification with 10% trifluoroacetic acid, followed by purification using the HiPPR Detergent Removal Kit (Thermo Fisher Scientific) and Pierce Peptide Desalting Spin Columns (Thermo Fisher Scientific) according to the manufacturer's instructions.

Liquid chromatography-mass spectrometry (LC-MS) analysis was performed on an Orbitrap Fusion Tribrid Mass Spectrometer interfaced with Easy-nLC1200 Liquid Chromatography System (Thermo Fisher Scientific). Peptides were trapped on an Acclaim Pepmap 100 C18 Trap Column (100 μm×2 cm, particle

size 5 μm; Thermo Fischer Scientific) and separated on an in-house packed analytical column (75 μm×35 cm, particle size 3 μm, Reprosil-Pur C18; Dr. Maisch, Ammerbuch, Germany) using a stepped gradient from 5–80% acetonitrile in 0.2% formic acid over 90 min at a flow of 300 nl/min. MS/MS was operated in a data-dependent mode where the precursor ion mass spectra were acquired at a resolution of 120,000 and an m/z range of 375 to 1,500. Using a cycle time of 3 s, the most abundant precursors with charge states 2 to 6 were isolated with an m/z window of 0.7 and fragmented by higher-energy collisional dissociation (HCD) at 30%. Fragment spectra were recorded in the Orbitrap with a resolution of 30,000 and a maximum injection time of 110 ms.

Data analysis was performed using Proteome Discoverer (2.4v; Thermo Fisher Scientific). Identification was executed using Mascot (2.5.1v; Matrix Science, London, UK) as search engine by matching against the *Homo sapiens* database of SwissProt (May 2022; 20,379 entries). The precursor mass tolerance was set to 5 ppm and fragment mass tolerance to 0.6 Da. Tryptic peptides were accepted with zero missed cleavage; methionine oxidation was selected as variable modification and cysteine methylthiolation was set as fixed modification. Fixed Value PSM Validator was used for validation with a maximum DeltaCn of 5%. Only unique peptides were used for quantification and proteins identified by less than two unique peptides were excluded from further analysis. The fold change > 3 and $P < 0.005$ based on median protein abundances comparing HepG2 cells transfected with *MYC-MST3* or *MYC-MST4 versus* an empty control plasmid (n = 4) were applied as the threshold parameters to identify interacting proteins.

Statistical Analysis

Statistical significance between the groups was evaluated using one-way ANOVA with a two-sample Student's *t*-test for post hoc analysis. Differences were considered statistically significant at $P < 0.05$. All statistical analyses were performed using SPSS statistics (24v; IBM Corporation, Armonk, NY).

The HCC samples extracted from TCGA were divided into high-expression and low-expression groups based on the median expression value of *MST3* or *MST4*. The survival data of HCC patients from the TCGA database was evaluated using the "survival" (3.2-10v) R package (statistical analysis of survival data) and "survminer" (0.4.9v) R package (visualization) (39) for the prognostic analysis according to the Kaplan-Meier method. The ssGSEA algorithm in the "GSVA" (1.34.0v) R package (40) was used to evaluate the tumor infiltration status of 19 immune cell types (41). The Spearman's correlation analysis was further performed to determine the relationship between expression levels of *MST3* and *MST4* and the immune cell infiltration status.

Results

Expression of MST3 and MST4 Correlates with the Progression of HCC

By analyzing the microarray GEO datasets of two large cohorts (GSE14520: n = 225 for tumor and n = 220 for nontumor; GSE36376: n = 240 for tumor and n = 193 for nontumor) and the whole RNA-seq data

combing TCGA and GTEx (n = 371 for tumor and n = 160 for nontumor), we found that gene expression of MST3 and MST4 was markedly higher in human HCC tissues compared with the nontumor controls (Fig. 1A-C). Moreover, in the subset of 50 paired samples from the TCGA database, *MST3* and *MST4* were elevated in HCC tumors compared to the adjacent nontumor tissues (Fig. 1D). Notably, we detected a positive correlation between hepatic *MST3* and *MST4* expression in HCC subjects (Fig. 1E).

To further understand the role of these kinases in the progression of HCC, we examined the correlation between *MST3/MST4* levels and the clinicopathological features of HCC patients from the TCGA database. Serum AFP has been identified as a prognostic marker of HCC shown to associate with tumor aggressiveness (size, multinodular appearance, and vascular invasion) (42–45). Here we found that high hepatic levels of *MST3* and *MST4* in HCC patients were accompanied by up-regulated serum AFP and advanced histological HCC grades (Fig. 1F-G). Consistently, Kaplan-Meier survival curve analysis showed that HCC subjects with a relatively high *MST*4 expression presented a significantly lower overall survival (Fig. 1H), disease-specific survival (Fig. 1I), and progress-free interval (Fig. 1J) compared to those with a low *MST4* expression level. No relationship between *MST3* abundance and survival outcomes was identified in HCC patients (data not shown).

Next, we analyzed the immune microenvironment of tumor tissue in HCC subjects from the TCGA database by ssGSEA (Supplementary Figure S2). We found that hepatic *MST3* and *MST4* transcripts displayed highest negative correlation with cytotoxic cells (ρ=-0.292, $P < 0.001$ for MST3; ρ=-0.161, $P = 0.002$ for MST4) and highest positive correlation with T helper cells (ρ = 0.437, $P < 0.001$ for MST3; ρ = 0.344, $P < 0.001$ for MST4).

To confirm the results from the bioinformatics assessment of the online databases, we analyzed the expression of *MST3* and *MST4* mRNA in liver biopsies from an independent cohort of HCC patients (n = 48) and control subjects (n = 214). Importantly, while the etiology of HCC in the online databases was not known, the patients with hepatitis B and C virus infection were excluded in this cohort, suggesting that the HCC development was likely triggered by NASH. Consistent with a metabolic origin of HCC, these patients displayed increased hepatic abundance of NASH markers collagen type I alpha 1 chain (*COL1A1*) and transforming growth factor beta 1 (*TGFB1*) compared with controls (Fig. 1K), elevated fasting blood glucose (114 ± 6.1 *versus* 95 ± 2.6 mg/dl, $P = 0.009$; available in a subgroup of 92 subjects), and a relatively high BMI (25.8 ± 0.6 *versus* 25.4 ± 0.3 kg/m^2; no difference between the groups). We found that, even in this cohort, the mRNA levels of MST3 and MST4 were up-regulated in liver biopsies from HCC patients compared with the control subjects (Fig. 1L). Furthermore, we observed that transcripts of these two kinases positively correlated with hepatic mRNA abundance of markers of poor HCC prognosis vimentin (*VIM*), *EPCAM*, catenin beta 1 (*CTNNB1*), and glypican 3 (*GPC3;* Supplementary Figure S3). Of note, there was no correlation between the expression of *MST3* and *MST4* mRNA and *AFP* (Supplementary Figure S3). It should be emphasized that the HCC patients were slightly older than the subjects in the control group (67 ± 1.7 *versus* 62 ± 0.8 years). However, neither age nor fasting blood glucose were associated with the expression of *MST3* and *MST4* mRNA ($P > 0.7$) and the difference

between the groups was independent of age and plasma glucose concentrations as analyzed by a multivariate model (data not shown).

MST3 and MST4 Control the Proliferation and Apoptosis of Human HCC Cells in Vitro

To explore the biological effect of MST3 and MST4 single knockdown on tumorigenesis of human HCC cells, and to compare this to the simultaneous silencing of both kinases, we transfected HepG2 cell line with *MST3*-, *MST4*-, or *MST3*/*MST4*-specific siRNA *versus* a non-targeting control (NTC) siRNA. As expected, the target mRNA and protein levels were efficiently down-regulated in cells transfected with the corresponding siRNA (Fig. 2A-B). Notably, the silencing of MST3 had no impact on the protein abundance of MST4; however, we detected a slight but significant increase in the mRNA and protein expression of MST3 in MST4-deficient HepG2 cells (Fig. 2A-B).

To examine the impact of MST3 and MST4 on the proliferation of hepatocytes, we performed the colony formation and EdU labeling assays. EdU experiments revealed markedly suppressed proliferation of MST3-, MST4-, or MST3/MST4-deficient HepG2 cells (Fig. 2C), which was consistent with a significant decrease in colony formation rates (Fig. 2D). In addition, the abundance of four different markers of hepatocyte proliferation – PCNA, Ki67, CK19, and cyclin D1– was markedly down-regulated in HepG2 cells where MST3, MST4, or MST3/MST4 were depleted, in parallel with significantly increased levels of p27 protein, which is known to block cancer cell proliferation and induce cell cycle arrest (Fig. 2E-F)(46). We did not detect any differences in viability comparing HepG2 cells transfected with *MST3*, *MST4*, or *MST3*/*MST4* siRNA *versus* NTC siRNA (Fig. 2G).

Both MST3 and MST4 have been reported to induce apoptosis in HEK293 (human embryonic kidney) and HeLa (human cervical cancer) cells (47–50). Here, we found that the expression of the proapoptotic proteins CASP3 and BAX was decreased in MST3-, MST4-, or MST3/MST4-deficient HepG2 cells (Fig. 3A-B). The quantification of Apopxin Violet labeling also revealed a slightly lower rate of initial/intermediate stages of apoptosis in HepG2 cells transfected with *MST3*, *MST4*, or *MST3*/*MST4* siRNA (Fig. 3C).

Similar to these observations in HepG2, we found that the silencing of MST3 and/or MST4 significantly reduced the proliferation and apoptosis of Hep3B cells (Supplementary Figure S4*A-D*). We did not detect any differences in viability comparing Hep3B cells transfected with *MST3*, *MST4*, or *MST3*/*MST4* siRNA *versus* NTC siRNA (Supplementary Figure S4*E*).

Knockdown of MST3 and MST4 Suppresses the Migration, Invasion, and Epithelial-Mesenchymal Transition (EMT) of Human HCC Cells

To evaluate the impact of MST3 and MST4 on cell motility, we performed transwell migration and scratch assays in hepatocytes. We found that the silencing of MST3, MST4, or MST3/MST4 significantly suppressed the migration of HepG2 cells in both these assays (Fig. 4A-B). Considering the central role of invasion in the progression of HCC (51, 52), the transwell assay was modified by coating the chambers

with Matrigel to evaluate the role of these kinases in cell invasiveness. Results showed that the knockdown of MST3, MST4, or MST3/MST4 notably blocked the invasion ability of HepG2 cells (Fig. 4D). Additionally, the abundance of migration-, invasion-, and EMT-associated factors, including matrix metalloprotein 2 (MMP2), matrix metalloprotein 9 (MMP9), N-cadherin, and fibronectin was reduced in MST3-, MST4, or MST3/MST4-deficient cells, while the expression of the epithelial marker E-cadherin was strengthened (Fig. 4C,E). Consistently, HepG2 cells transfected with *MST3*, *MST4*, or *MST3/MST4* siRNA exhibited an epithelial-like morphology with a cobblestone-like growth pattern, whereas cells transfected with NTC siRNA displayed a mesenchymal-like phenotype with a spreading growth pattern (Fig. 4F). Immunofluorescent microscopy assessment further demonstrated that MST3-, MST4-, or MST3/MST4-deficient HepG2 cells presented lower levels of EpCAM, AFP, GRP78, and YAP (Fig. 5), which are markers associated with poor prognosis and aggravated invasion and migration of human HCC (53–57).

In line with these observations in HepG2, we found that the silencing of MST3 and/or MST4 kinases suppressed the migratory and invasive capacity as well as EMT of Hep3B cells (Supplementary Figure S5).

Silencing of MST3 and MST4 Signaling Alters the Pro-Oncogenic Pathways in Human HCC Cells

To explore the mechanisms by which MST3 and MST4 impact on hepatocellular carcinogenesis, we monitored the activation of mitogen-activated protein kinases (MAPKs) extracellular signal-regulated kinase 1/2 (ERK1/2) and Jun N-terminal kinase (JNK1/2), which are important signaling components controlling proliferation and migration in human HCC (58). We detected no difference in total or phospho-ERK1/2 (Thr^{202}/Tyr^{204}), or total or phospho-JNK1/2 (Thr^{183}/Tyr^{185}), in HepG2 cells transfected with *MST3*, *MST4*, or *MST3/MST4* siRNA *versus* NTC siRNA (Fig. 6A-B). YAP activation is an independent prognostic marker in HCC and loss of YAP signaling has been shown to impair the migration and invasion of human HCC cells (57, 59). We found that the protein abundance of YAP was about 2-fold higher in MST3, MST4, or MST3/MST4-deficient HepG2 cells and the levels of phospho-YAP (Ser^{127}; inactive form) were also elevated to a comparable degree without any change in the phospho-YAP/YAP ratio (Fig. 6C). MST4 has previously been described to activate autophagy-related gene 4B (ATG4B) via phosphorylation of the Ser^{383} residue (21). Notably, ATG4B has also been implicated in survival and growth of HCC cells (60, 61). Here, we did not detect any alteration in the phosphorylation level of ATG4B (Ser^{383}), or in the phospho-ATG4B/ATG4B ratio, in HepG2 cells where MST3, MST4, or MST3/MST4 were knocked down (Fig. 6D). STAT3 signaling is known to be activated in human HCC and hepatocyte-specific STAT3 ablation has been shown to prevent HCC development (62, 63). Interestingly, we found that the phosphorylation of STAT3 (Thr^{705}; active form), but not the total protein abundance, was significantly lower in MST3-, MST4, or MST3/MST4-deficient HepG2 cells (Fig. 6E).

To discover the hepatocellular interaction partners of MST3 and MST4, we performed anti-MYC immunoprecipitation in HepG2 cells transfected with plasmids encoding *MYC-MST3* or *MYC-MST4*,

followed by mass spectrometry analysis (Fig. 7A). We identified Golgi-associated protein GOLGA2 (also known as GM130) and several components of the striatin (STRN)-interacting phosphatase and kinase (STRIPAK) complex as binding partners for both MST3 and MST4 (Fig. 7B). To this end, the association of MST3/MST4 with GOLGA2 and STRIPAK has been previously reported in several cell lines such as HEK293 and HeLa (64–68). It is also known that, in mammalian STRIPAK complexes, the STRN family members bind MST3 and MST4 via the stabilizing scaffold programmed cell death 10 (PDCD10; also known as CCM3 or TFAR15) and orchestrate the dephosphorylation and inactivation of MST3 and MST4 by STRN-associated phosphatase 2A (PP2A) (Fig. 7C) (69). In addition, we detected an interaction between MST3 and retinoblastoma-binding protein 4 (RBBP4; also known as RBAP48), transglutaminase 2 (TGM2), and leucine-rich PPR motif-containing protein (LRPPRC; also known as LRP130) in HepG2 cells (Fig. 7B; Supplementary Table S3).

Discussion

In this study, we show that STE20-type kinases *MST3* and *MST4* were up-regulated in human HCC tissues, and the silencing of MST3 or MST4 suppressed tumorigenicity of human HCC cell lines. Together, our data provide the first evidence that MST3 and MST4 proteins may function as oncogenes in the development of HCC, a cancer type with heavy disease burden and poor prognosis.

This report provides consistent evidence that proliferation, migration, invasion, and EMT abilities were markedly reduced in MST3 or MST4-deficient HCC cells (Fig. 8); however, the mode-of-action of these kinases remains elusive. Interestingly, we found that the silencing of MST3 or MST4 resulted in decreased phosphorylation of STAT3, a critical regulator of hepatocarcinogenesis (62, 63). Furthermore, we show that both MST3 and MST4 interacted with GOLGA2 and STRIPAK complex in HCC cells. It has been previously reported that the abundance of GOLGA2 and STRIPAK is upregulated in human HCC tumors compared with the adjacent nontumor tissue (70, 71). PDCD10 has also been demonstrated to promote the proliferation, migration, invasion, and EMT of human HCC cells *in vitro* and to aggravate tumor growth and metastasis in a mouse liver orthotopic xenograft model *in vivo* (72). In addition, we detected an interaction between MST3 and RBBP4, TGM2, and LRPPRC proteins, which are all implicated in the control of HCC development (73–75). Thus, it is plausible that inhibition of STAT3 signaling, and binding to different interaction partners, may be part of the mechanism by which MST3 and MST4 promote hepatocarcinogenesis. However, the architecture and regulation of these interactions, and the molecular pathways through which MST3/MST4 complexes control different cellular processes, remain unknown.

In this study, the silencing of MST3 in human HCC cells phenocopied the knockdown of MST4, resulting in a similar degree of inhibition in the cell proliferation, migration, invasion, and EMT. Clearly, our results show that the presence of MST4 protein in MST3-deficient HCC cells could not compensate for the loss of MST3, and *vice versa*, implying overlapping but non-redundant roles of these two kinases in the regulation of hepatocellular tumorigenicity. We also found that the combined depletion of MST3 and MST4 did not result in any consistent and significant benefit in terms of suppressed hepatocellular

proliferation, migration, invasion, and EMT, as compared with the knockdown of MST3 or MST4 individually. The lack of additive or synergistic effects in HCC cells transfected with both *MST3* and *MST4* siRNA suggests that these two kinases operate in the same pathway and/or employ a shared mechanism not augmented by combined depletion. Another possible explanation involves a ceiling effect in the repression the hepatocellular tumorigenesis by MST3 and MST4. Interestingly, we did not detect any interaction between these two kinases in human hepatocytes, although MST3 and MST4 have been shown to directly interact in HEK293 cells (76).

It is important to emphasize that all the *in vitro* investigations in this report were carried out using immortalized human cell lines (HepG2 and Hep3B), which may not fully replicate the *in vivo* milieu. To this end, further experiments using mouse models and human primary cells are warranted.

Before this report, we have provided several layers of evidence supporting the critical function of MST3 and MST4 kinases in the development and progression of NASH (10–12). However, the data on the potential role of these proteins in HCC have remained controversial as MST4 was described to display both pro- and anti-HCC effects (15–17) while MST3 has not previously been implicated in HCC pathology. Here, we show that inactivation of both MST3 and MST4, but also either of them individually, markedly suppressed the tumorigenesis of human HCC cells. Notably, the combined silencing of MST3 and MST4 displayed no additive or synergistic impact on hepatocellular tumorigenesis, indicating that these kinases act in the same signaling pathway, although the hierarchy, upstream regulators, and downstream targets remain elusive. Together, our study supports the oncogenic effect of MST3 and MST4 in human HCC and suggests that targeting these kinases may provide a novel strategy for the treatment of liver cancer.

Declarations

ACKNOWLEDGEMENTS: The authors thank Carina Sihlbom and the Proteomics Core Facility at Sahlgrenska Academy, University of Gothenburg, for the relative quantification using LC-MS/MS.

AUTHOR CONTRIBUTIONS: M.C. generated the bulk of the results and wrote the manuscript. Y.X. contributed to the research data and wrote the manuscript. S.K.A., E.C., and E.A. contributed to the research data. H.-U.M. provided expertise and contributed to the discussion. A.P. carried out qRT-PCR in human liver biopsies and provided expertise and contributed to the discussion. M.M. directed the project, designed the study, interpreted the data, and wrote the manuscript. All the authors revised the article critically for important intellectual content and approved the final version of the article to be published.

FUNDING: This work was supported by grants from the Swedish Research Council, the Swedish Cancer Society, the Novo Nordisk Foundation, the Swedish Heart-Lung Foundation, the Swedish Diabetes Foundation, the Å. Wiberg Foundation, the Adlerbert Research Foundation, the I. Hultman Foundation, the F. Neubergh Foundation, the Prof. N. Svartz Foundation, the L. and J. Grönberg Foundation, the W. and M. Lundgren Foundation, the I.-B. and A. Lundberg Research Foundation, the Erling-Persson Foundation, the Wenner-Gren Foundation, and by the Swedish state under the agreement between the Swedish Government and the county councils, the ALF-agreement.

DATA AVAILABILITY: All data related to this study are available within the article and its Supplementary information files. Gene expression data for this study are available from TCGA, GTEx, and two HCC datasets (GSE14520 and GSE36376) from the GEO database.

Ethical approval and consent to participate: The study was conducted according to the guidelines of the Declaration of Helsinki, and approved by the Ethics Committee of the University of Tübingen, Germany (368/2012BO2).

Consent for publication: All authors have agreed to publish this manuscript.

Competing interests: The authors declare no conflict of interest.

References

1. Vogel A, Meyer T, Sapisochin G, Salem R, and Saborowski A. Hepatocellular carcinoma. *Lancet.* 2022;400(10360):1345-62.
2. Cramer T, and Vaupel P. Severe hypoxia is a typical characteristic of human hepatocellular carcinoma: Scientific fact or fallacy? *J Hepatol.* 2022;76(4):975-80.
3. Chen Q, Shu C, Laurence AD, Chen Y, Peng BG, Zhen ZJ, et al. Effect of Huaier granule on recurrence after curative resection of HCC: a multicentre, randomised clinical trial. *Gut.* 2018;67(11):2006-16.
4. Llovet JM, Kelley RK, Villanueva A, Singal AG, Pikarsky E, Roayaie S, et al. Hepatocellular carcinoma. *Nat Rev Dis Primers.* 2021;7(1):6.
5. Ioannou GN. Epidemiology and risk-stratification of NAFLD-associated HCC. *J Hepatol.* 2021;75(6):1476-84.
6. Huang DQ, Singal AG, Kono Y, Tan DJH, El-Serag HB, and Loomba R. Changing global epidemiology of liver cancer from 2010 to 2019: NASH is the fastest growing cause of liver cancer. *Cell Metab.* 2022;34(7):969-77.
7. Singal AG, Lampertico P, and Nahon P. Epidemiology and surveillance for hepatocellular carcinoma: New trends. *J Hepatol.* 2020;72(2):250-61.
8. Sheka AC, Adeyi O, Thompson J, Hameed B, Crawford PA, and Ikramuddin S. Nonalcoholic Steatohepatitis: A Review. *JAMA.* 2020;323(12):1175-83.
9. Samuel VT, and Shulman GI. Nonalcoholic Fatty Liver Disease as a Nexus of Metabolic and Hepatic Diseases. *Cell Metab.* 2019;27(1):22-41.
10. Cansby E, Kulkarni NM, Magnusson E, Kurhe Y, Amrutkar M, Nerstedt A, et al. Protein kinase MST3 modulates lipid homeostasis in hepatocytes and correlates with nonalcoholic steatohepatitis in humans. *FASEB J.* 2019;33(9):9974-89.
11. Caputo M, Cansby E, Kumari S, Kurhe Y, Nair S, Stahlman M, et al. STE20-Type Protein Kinase MST4 Controls NAFLD Progression by Regulating Lipid Droplet Dynamics and Metabolic Stress in Hepatocytes. *Hepatol Commun.* 2021;5(7):1183-200.

12. Caputo M, Kurhe Y, Kumari S, Cansby E, Amrutkar M, Scandalis E, et al. Silencing of STE20-type kinase MST3 in mice with antisense oligonucleotide treatment ameliorates diet-induced nonalcoholic fatty liver disease. *FASEB J.* 2021;35(5):e21567.
13. Mashek DG, Khan SA, Sathyanarayan A, Ploeger JM, and Franklin MP. Hepatic lipid droplet biology: Getting to the root of fatty liver. *Hepatology.* 2015;62(3):964-7.
14. Gluchowski NL, Becuwe M, Walther TC, and Farese RV, Jr. Lipid droplets and liver disease: from basic biology to clinical implications. *Nat Rev Gastroenterol Hepatol.* 2017;14(6):343-55.
15. Lin ZH, Wang L, Zhang JB, Liu Y, Li XQ, Guo L, et al. MST4 promotes hepatocellular carcinoma epithelial-mesenchymal transition and metastasis via activation of the p-ERK pathway. *Int J Oncol.* 2014;45(2):629-40.
16. Dian MJ, Li J, Zhang XL, Li ZJ, Zhou Y, Zhou W, et al. MST4 negatively regulates the EMT, invasion and metastasis of HCC cells by inactivating PI3K/AKT/Snail1 axis. *J Cancer.* 2021;12(15):4463-77.
17. Hao WC, Zhong QL, Pang WQ, Dian MJ, Li J, Han LX, et al. MST4 inhibits human hepatocellular carcinoma cell proliferation and induces cell cycle arrest via suppression of PI3K/AKT pathway. *J Cancer.* 2020;11(17):5106-17.
18. Li T, Deng L, He X, Jiang G, Hu F, Ye S, et al. MST4 Predicts Poor Prognosis And Promotes Metastasis By Facilitating Epithelial-Mesenchymal Transition In Gastric Cancer. *Cancer Manag Res.* 2019;11:9353-69.
19. Lee KT, Chang CL, Li CY, Song H, Shan YS, and Lai MD. The oncogenic role of MST3 in human gastric cancer. *Am J Cancer Res.* 2018;8(10):2130-39.
20. Chen M, Zhang H, Shi Z, Li Y, Zhang X, Gao Z, et al. The MST4-MOB4 complex disrupts the MST1-MOB1 complex in the Hippo-YAP pathway and plays a pro-oncogenic role in pancreatic cancer. *J Biol Chem.* 2018;293(37):14455-69.
21. Huang T, Kim CK, Alvarez AA, Pangeni RP, Wan X, Song X, et al. MST4 Phosphorylation of ATG4B Regulates Autophagic Activity, Tumorigenicity, and Radioresistance in Glioblastoma. *Cancer Cell.* 2017;32(6):840-55.
22. Zhang H, Lin M, Dong C, Tang Y, An L, Ju J, et al. An MST4-pbeta-Catenin(Thr40) Signaling Axis Controls Intestinal Stem Cell and Tumorigenesis. *Adv Sci (Weinh).* 2021;8(17):e2004850.
23. Madsen CD, Hooper S, Tozluoglu M, Bruckbauer A, Fletcher G, Erler JT, et al. STRIPAK components determine mode of cancer cell migration and metastasis. *Nat Cell Biol.* 2015;17(1):68-80.
24. Zhang H, Ma X, Peng S, Nan X, and Zhao H. Differential expression of MST4, STK25 and PDCD10 between benign prostatic hyperplasia and prostate cancer. *Int J Clin Exp Pathol.* 2014;7(11):8105-11.
25. Arora R, Kim JH, Getu AA, Angajala A, Chen YL, Wang B, et al. MST4: A Potential Oncogene and Therapeutic Target in Breast Cancer. *Cells.* 2022;11(24):4057.
26. Shi X, Zou J, Wang Y, Zhao J, Ye B, Qi Q, et al. MST4 as a novel therapeutic target for autophagy and radiosensitivity in gastric cancer. *IUBMB Life.* 2022;75(2):117-36.

27. Zhang Y, Tang W, Zhang H, Niu X, Xu Y, Zhang J, et al. A network of interactions enables CCM3 and STK24 to coordinate UNC13D-driven vesicle exocytosis in neutrophils. *Dev Cell.* 2013;27(2):215-26.
28. Sartages M, Garcia-Colomer M, Iglesias C, Howell BW, Macia M, Pena P, et al. GCKIII (Germinal Center Kinase III) Kinases STK24 and STK25 (Serine/Threonine Kinase 24 and 25) Inhibit Cavernoma Development. *Stroke.* 2022;53(3):976-86.
29. Ceccarelli DF, Laister RC, Mulligan VK, Kean MJ, Goudreault M, Scott IC, et al. CCM3/PDCD10 heterodimerizes with germinal center kinase III (GCKIII) proteins using a mechanism analogous to CCM3 homodimerization. *J Biol Chem.* 2011;286(28):25056-64.
30. Tang J, Ip JP, Ye T, Ng YP, Yung WH, Wu Z, et al. Cdk5-dependent Mst3 phosphorylation and activity regulate neuronal migration through RhoA inhibition. *J Neurosci.* 2014;34(22):7425-36.
31. Ultanir SK, Yadav S, Hertz NT, Oses-Prieto JA, Claxton S, Burlingame AL, et al. MST3 kinase phosphorylates TAO1/2 to enable Myosin Va function in promoting spine synapse development. *Neuron.* 2014;84(5):968-82.
32. Matsuki T, Iio A, Ueda M, Tsuneura Y, Howell BW, and Nakayama A. STK25 and MST3 Have Overlapping Roles to Regulate Rho GTPases during Cortical Development. *J Neurosci.* 2021;41(43):8887-903.
33. Jiao S, Zhang Z, Li C, Huang M, Shi Z, Wang Y, et al. The kinase MST4 limits inflammatory responses through direct phosphorylation of the adaptor TRAF6. *Nat Immunol.* 2015;16(3):246-57.
34. Shi Z, and Zhou Z. MST kinases in innate immune signaling. *Cell Stress.* 2017;2(1):4-13.
35. Cancer Genome Atlas Research N, Weinstein JN, Collisson EA, Mills GB, Shaw KR, Ozenberger BA, et al. The Cancer Genome Atlas Pan-Cancer analysis project. *Nat Genet.* 2013;45(10):1113-20.
36. Consortium GT. The Genotype-Tissue Expression (GTEx) project. *Nat Genet.* 2013;45(6):580-5.
37. Cansby E, Amrutkar M, Manneras Holm L, Nerstedt A, Reyahi A, Stenfeldt E, et al. Increased expression of STK25 leads to impaired glucose utilization and insulin sensitivity in mice challenged with a high-fat diet. *FASEB J.* 2013;27(9):3660-71.
38. Wisniewski JR, Zougman A, Nagaraj N, and Mann M. Universal sample preparation method for proteome analysis. *Nat Methods.* 2009;6(5):359-62.
39. Liu J, Lichtenberg T, Hoadley KA, Poisson LM, Lazar AJ, Cherniack AD, et al. An Integrated TCGA Pan-Cancer Clinical Data Resource to Drive High-Quality Survival Outcome Analytics. *Cell.* 2018;173(2):400-16.
40. Hanzelmann S, Castelo R, and Guinney J. GSVA: gene set variation analysis for microarray and RNA-seq data. *BMC Bioinformatics.* 2013;14:7.
41. Bindea G, Mlecnik B, Tosolini M, Kirilovsky A, Waldner M, Obenauf AC, et al. Spatiotemporal dynamics of intratumoral immune cells reveal the immune landscape in human cancer. *Immunity.* 2013;39(4):782-95.
42. Sudan D, Chapman WC, Cameron JL, and Agopian V. A Novel Prognostic Nomogram Accurately Predicts Hepatocellular Carcinoma Recurrence after Liver Transplantation: Analysis of 865

Consecutive Liver Transplant Recipients Discussion. *J Am Coll Surgeons.* 2015;220(4):427-9.

43. Berry K, and Ioannou GN. Serum alpha-fetoprotein level independently predicts posttransplant survival in patients with hepatocellular carcinoma. *Liver Transplant.* 2013;19(6):634-45.
44. Duvoux C, Roudot-Thoraval F, Decaens T, Pessione F, Badran H, Piardi T, et al. Liver transplantation for hepatocellular carcinoma: a model including alpha-fetoprotein improves the performance of Milan criteria. *Gastroenterology.* 2012;143(4):986-94.
45. Giannini EG, Sammito G, Farinati F, Ciccarese F, Pecorelli A, Rapaccini GL, et al. Determinants of alpha-fetoprotein levels in patients with hepatocellular carcinoma: implications for its clinical use. *Cancer.* 2014;120(14):2150-7.
46. Luo Y, Gao Y, Liu W, Yang Y, Jiang J, Wang Y, et al. Myelocytomatosis-Protein Arginine N-Methyltransferase 5 Axis Defines the Tumorigenesis and Immune Response in Hepatocellular Carcinoma. *Hepatology.* 2021;74(4):1932-51.
47. Huang CY, Wu YM, Hsu CY, Lee WS, Lai MD, Lu TJ, et al. Caspase activation of mammalian sterile 20-like kinase 3 (Mst3). Nuclear translocation and induction of apoptosis. *J Biol Chem.* 2002;277(37):34367-74.
48. Lee WS, Hsu CY, Wang PL, Huang CY, Chang CH, and Yuan CJ. Identification and characterization of the nuclear import and export signals of the mammalian Ste20-like protein kinase 3. *FEBS Lett.* 2004;572(1-3):41-5.
49. Shi Z, Jiao S, Zhang Z, Ma M, Zhang Z, Chen C, et al. Structure of the MST4 in complex with MO25 provides insights into its activation mechanism. *Structure.* 2013;21(3):449-61.
50. Ma X, Zhao H, Shan J, Long F, Chen Y, Chen Y, et al. PDCD10 interacts with Ste20-related kinase MST4 to promote cell growth and transformation via modulation of the ERK pathway. *Mol Biol Cell.* 2007;18(6):1965-78.
51. Fan ST. Hepatocellular carcinoma-resection or transplant? *Nat Rev Gastro Hepat.* 2012;9(12):732-7.
52. Zimmermann A. Invasion Patterns and Metastatic Patterns of Hepatocellular Carcinoma. *Tumors and Tumor-Like Lesions of the Hepatobiliary Tract.* 2016:91-119.
53. Terris B, Cavard C, and Perret C. EpCAM, a new marker for cancer stem cells in hepatocellular carcinoma. *Journal of Hepatology.* 2010;52(2):280-1.
54. Teufel M, Seidel H, Kochert K, Meinhardt G, Finn RS, Llovet JM, et al. Biomarkers Associated With Response to Regorafenib in Patients With Hepatocellular Carcinoma. *Gastroenterology.* 2019;156(6):1731-41.
55. Halazun KJ, Rosenblatt RE, Mehta N, Lai Q, Hajifathalian K, Gorgen A, et al. Dynamic alpha-Fetoprotein Response and Outcomes After Liver Transplant for Hepatocellular Carcinoma. *JAMA Surg.* 2021;156(6):559-67.
56. Luo C, Xiong H, Chen L, Liu X, Zou S, Guan J, et al. GRP78 Promotes Hepatocellular Carcinoma proliferation by increasing FAT10 expression through the NF-kappaB pathway. *Exp Cell Res.* 2018;365(1):1-11.

57. Shi C, Cai Y, Li Y, Li Y, Hu N, Ma S, et al. Yap promotes hepatocellular carcinoma metastasis and mobilization via governing cofilin/F-actin/lamellipodium axis by regulation of JNK/Bnip3/SERCA/CaMKII pathways. *Redox Biol.* 2018;14:59-71.
58. Min L, He B, and Hui L. Mitogen-activated protein kinases in hepatocellular carcinoma development. *Semin Cancer Biol.* 2011;21(1):10-20.
59. Russell JO, and Camargo FD. Hippo signalling in the liver: role in development, regeneration and disease. *Nat Rev Gastroenterol Hepatol.* 2022;19(5):297-312.
60. Ni Z, He J, Wu Y, Hu C, Dai X, Yan X, et al. AKT-mediated phosphorylation of ATG4B impairs mitochondrial activity and enhances the Warburg effect in hepatocellular carcinoma cells. *Autophagy.* 2018;14(4):685-701.
61. Toshima T, Shirabe K, Matsumoto Y, Yoshiya S, Ikegami T, Yoshizumi T, et al. Autophagy enhances hepatocellular carcinoma progression by activation of mitochondrial beta-oxidation. *J Gastroenterol.* 2014;49(5):907-16.
62. Calvisi DF, Ladu S, Gorden A, Farina M, Conner EA, Lee JS, et al. Ubiquitous activation of Ras and Jak/Stat pathways in human HCC. *Gastroenterology.* 2006;130(4):1117-28.
63. He G, Yu GY, Temkin V, Ogata H, Kuntzen C, Sakurai T, et al. Hepatocyte IKKbeta/NF-kappaB inhibits tumor promotion and progression by preventing oxidative stress-driven STAT3 activation. *Cancer Cell.* 2010;17(3):286-97.
64. Kean MJ, Ceccarelli DF, Goudreault M, Sanches M, Tate S, Larsen B, et al. Structure-function analysis of core STRIPAK Proteins: a signaling complex implicated in Golgi polarization. *J Biol Chem.* 2011;286(28):25065-75.
65. Preisinger C, Short B, De Corte V, Bruyneel E, Haas A, Kopajtich R, et al. YSK1 is activated by the Golgi matrix protein GM130 and plays a role in cell migration through its substrate 14-3-3zeta. *J Cell Biol.* 2004;164(7):1009-20.
66. Gordon J, Hwang J, Carrier KJ, Jones CA, Kern QL, Moreno CS, et al. Protein phosphatase 2a (PP2A) binds within the oligomerization domain of striatin and regulates the phosphorylation and activation of the mammalian Ste20-Like kinase Mst3. *BMC Biochem.* 2011;12:54.
67. Chen R, Xie R, Meng Z, Ma S, and Guan KL. STRIPAK integrates upstream signals to initiate the Hippo kinase cascade. *Nat Cell Biol.* 2019;21(12):1565-77.
68. Goudreault M, D'Ambrosio LM, Kean MJ, Mullin MJ, Larsen BG, Sanchez A, et al. A PP2A phosphatase high density interaction network identifies a novel striatin-interacting phosphatase and kinase complex linked to the cerebral cavernous malformation 3 (CCM3) protein. *Mol Cell Proteomics.* 2009;8(1):157-71.
69. Kuck U, Radchenko D, and Teichert I. STRIPAK, a highly conserved signaling complex, controls multiple eukaryotic cellular and developmental processes and is linked with human diseases. *Biol Chem.* 2019;400(8):1005-22.
70. Alcedo KP, Guerrero A, Basrur V, Fu D, Richardson ML, McLane JS, et al. Tumor-Selective Altered Glycosylation and Functional Attenuation of CD73 in Human Hepatocellular Carcinoma. *Hepatology*

Communications. 2019;3(10):1400-14.

71. Xie RL, Wen F, and Qin Y. The Dysregulation and Prognostic Analysis of STRIPAK Complex Across Cancers. *Front Cell Dev Biol.* 2020;8:625.
72. Sun B, Zhong FJ, Xu C, Li YM, Zhao YR, Cao MM, et al. Programmed cell death 10 promotes metastasis and epithelial-mesenchymal transition of hepatocellular carcinoma via PP2Ac-mediated YAP activation. *Cell Death & Disease.* 2021;12(9):849.
73. Ma H, Xie L, Zhang L, Yin X, Jiang H, Xie X, et al. Activated hepatic stellate cells promote epithelial-to-mesenchymal transition in hepatocellular carcinoma through transglutaminase 2-induced pseudohypoxia. *Commun Biol.* 2018;Oct 25(1:168)1:168.
74. Li WJ, Dai Y, Shi BY, Yue F, Zou J, Xu GB, et al. LRPPRC sustains Yap-P27-mediated cell ploidy and P62-HDAC6-mediated autophagy maturation and suppresses genome instability and hepatocellular carcinomas. *Oncogene.* 2020;39(19):3879-92.
75. Li L, Tang J, Zhang B, Yang W, LiuGao M, Wang R, et al. Epigenetic modification of MiR-429 promotes liver tumour-initiating cell properties by targeting Rb binding protein 4. *Gut.* 2015;64(1):156-67.
76. Cho NH, Cheveralls KC, Brunner AD, Kim K, Michaelis AC, Raghavan P, et al. OpenCell: Endogenous tagging for the cartography of human cellular organization. *Science.* 2022;375(6585).
77. Shi Z, Jiao S, and Zhou Z. STRIPAK complexes in cell signaling and cancer. *Oncogene.* 2016;35(35):4549-57.
78. Jeong BC, Bae SJ, Ni LS, Zhang XW, Bai XC, and Luo XL. Cryo-EM structure of the Hippo signaling integrator human STRIPAK. *Nat Struct Mol Biol.* 2021;28(3):290-299.

Figures

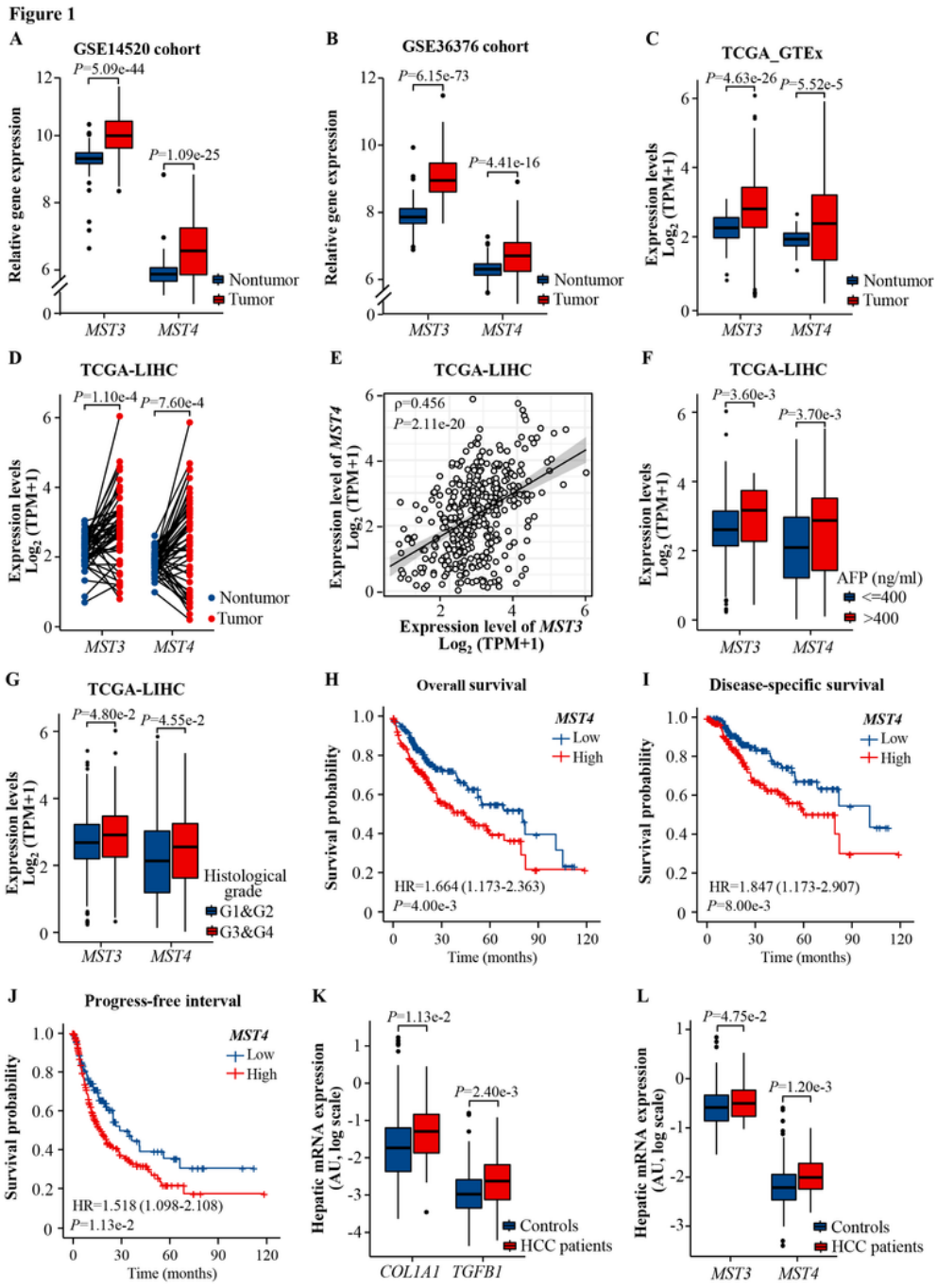

Figure 1

Expression of *MST3* and *MST4* mRNA in human liver biopsies positively correlates with the progression of HCC. (*A-C*) *MST3* and *MST4* mRNA expression in human HCC tissues compared with the nontumor controls obtained from the GSE14520 (*A*), GSE36376 (*B*), and combined TCGA and GTEx (*C*) datasets. (*D*) *MST3* and *MST4* mRNA expression in the subset of paired HCC tumors and adjacent nontumor samples. (*E*) Correlation between hepatic *MST3* and *MST4* mRNA expression in HCC subjects. (*F-G*)

MST3 and *MST4* mRNA expression in individuals with low *versus* high serum AFP concentration (*F*) and low *versus* high histological HCC grade (*G*). (*H-J*) Kaplan-Meier curves for overall (*H*) and disease-specific (*I*) survival as well as progress-free interval (*J*) in HCC patients with low *versus* high *MST4*expression. (*K-L*) Hepatic expression of NASH markers (*K*) as well as *MST3* and *MST4* (*L*) mRNA in an independent cohort of HCC patients and matched controls recruited at the University Hospital of Tübingen. mRNA expression was normalized to the endogenus control *RSP13*. For (*D-J*), data were acquired from the TCGA-LIHC dataset. For (*A-C*, *F-G*, and *K-L*), the box plots show the median (line in a box), first-to-third quartiles (boxes), 1.5× the interquartile range (whiskers), and outliers (dots). AU, arbitrary units; HR, hazard ratio; TPM, transcripts per kilobase million

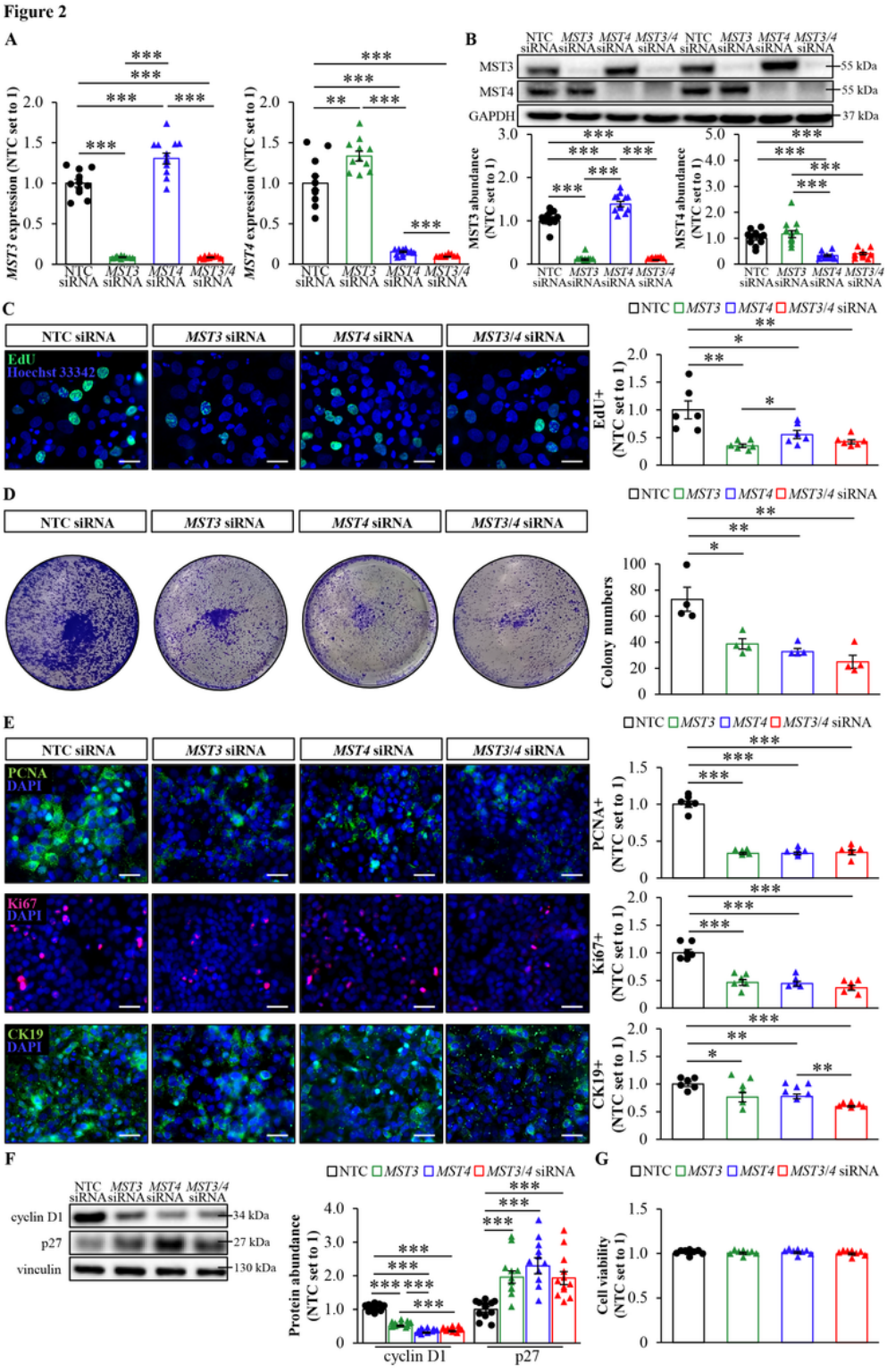

Figure 2

Silencing of MST3 and MST4 suppresses the proliferation of human HCC cells. HepG2 cellswere transfected with *MST3* and/or *MST4* siRNA, or NTC siRNA, and cultured with oleate supplementation.(*A-B*) MST3 and MST4 mRNA (*A*) and protein (*B*) abundance assessed by qRT-PCR and Western blot, respectively. In (*B*), protein levels analyzed by densitometry; representative Western blots are shown with glyceraldehyde-3-phosphate dehydrogenase (GAPDH) used as a loading control. (*C*)Representative

images of proliferating cells stained with EdU (green); nuclei stained with Hoechst 33342 (blue). The scale bars represent 25 µm. Quantification of the staining. (*D*) Representative images of colonies stained with crystal violet. Quantification of the number of colonies. (*E*) Representative images of cells processed for immunofluorescence with anti-PCNA (green), anti-Ki67 (pink), or anti-CK19 (green) antibodies; nuclei stained with DAPI (blue). The scale bars represent 25 µm. Quantification of the staining. (*F*) Cell lysates analyzed by Western blot using antibodies specific for cyclin D1 or p27. Protein levels analyzed by densitometry; representative Western blots are shown with vinculin used as a loading control. (*G*) Cell viability assessed using resazurin. Data are mean ± SEM from 3-6 (*C-E*) or 9-12 (*A-B*and *F-G*) wells per group. **P*<0.05, ***P*<0.01, ****P*<0.001

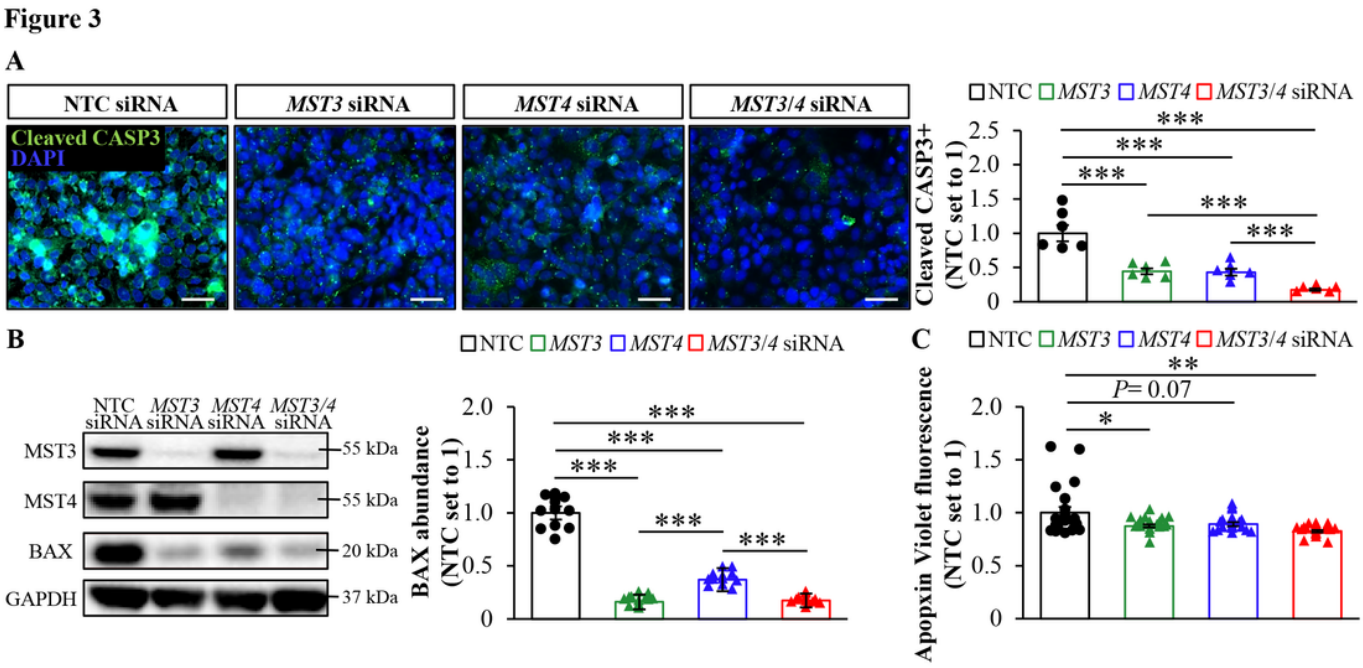

Figure 3

Knockdown of MST3 and MST4 protects human HCC cells from apoptosis. HepG2 cells were transfected with *MST3* and/or *MST4* siRNA, or NTC siRNA, and cultured with oleate supplementation. (*A*) Representative images of cells processed for immunofluorescence with anti-cleaved CASP3 (green) antibodies; nuclei stained with DAPI (blue). The scale bars represent 25 µm. Quantification of the staining. (*B*) Cell lysates analyzed by Western blot using antibodies specific for BAX, MST3, or MST4. Protein levels analyzed by densitometry; representative Western blots are shown with GAPDH used as a loading control. (*C*) Initial/intermediate stages of apoptosis monitored by staining with Apopxin Violet (Ex/Em = 405/450 nm). Data are mean ± SEM from 6 (*A*), 12 (*B*), or 20 (*C*) wells per group. **P*<0.05, ***P*<0.01, ****P*<0.001

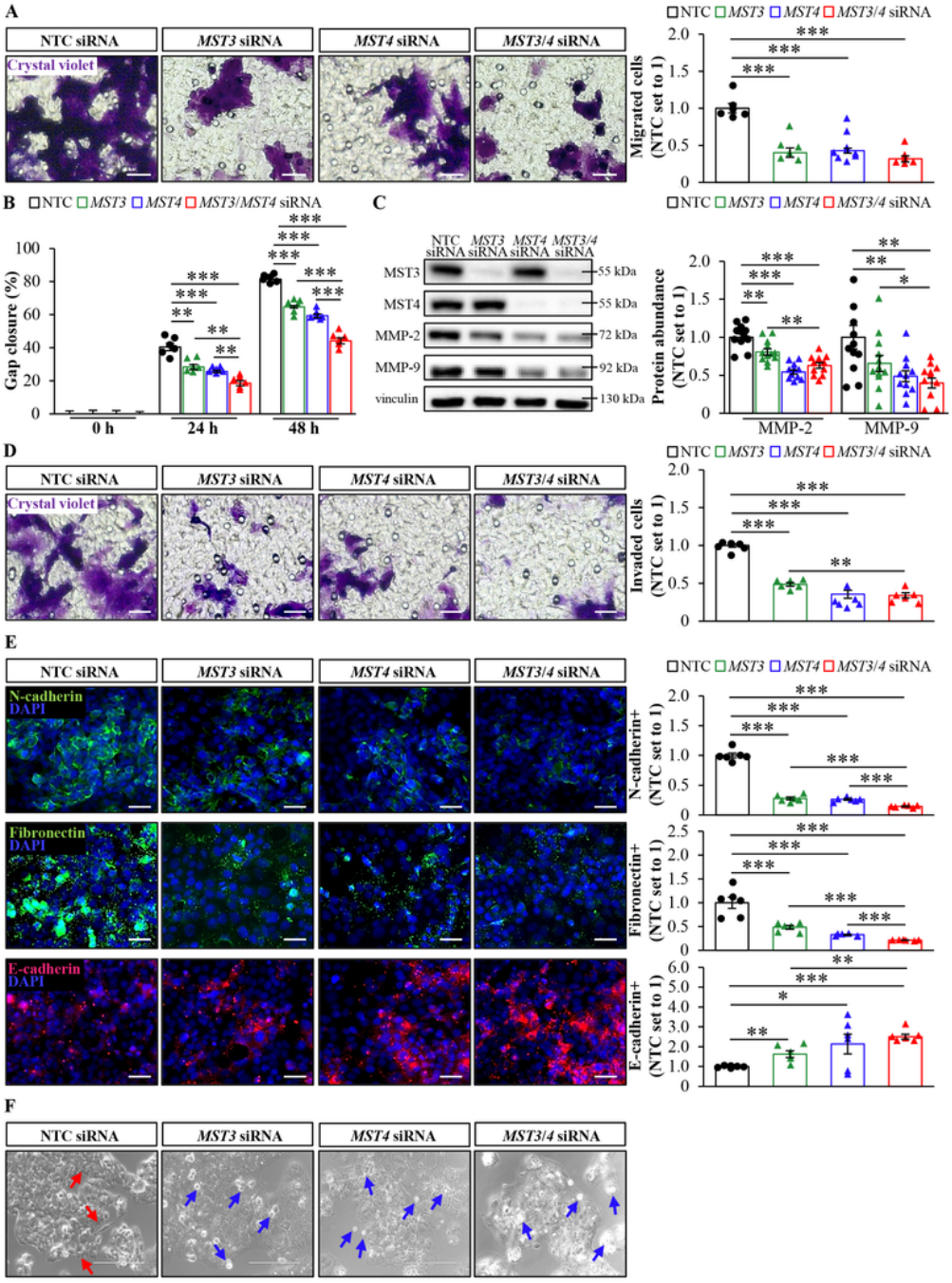

Figure 4

MST3 and MST4 control migration, invasion, and EMT of human HCC cells. HepG2 cells were transfected with *MST3*and/or *MST4* siRNA, or NTC siRNA, and cultured with oleate supplementation. (*A*) Representative images of migrated cells stained with crystal violet. The scale bars represent 25 μm. Quantification of the staining. (*B*) Scratch assay: gap closure was estimated at the indicated time points. (*C*) Cell lysates analyzed by Western blot using antibodies specific for MMP-2, MMP-9, MST3, or MST4.

Protein levels analyzed by densitometry; representative Western blots are shown with vinculin used as a loading control. (*D*) Representative images of invaded cells stained with crystal violet. The scale bars represent 25 µm. Quantification of the staining. (*E*) Representative images of cells processed for immunofluorescence with anti-N-cadherin (green), anti-fibronectin (green), or anti-E-cadherin (red) antibodies; nuclei stained with DAPI (blue). The scale bars represent 25 µm. Quantification of the staining. (*F*) Representative phase-contrast images showing cells with mesenchymal- (red arrows) and epithelial-like (blue arrows) morphology. The scale bars represent 200 µm. Data are mean ± SEM from 6-10 (*A-B*-and *D-E*) or 12 (*C*) wells per group. *P<0.05, **P<0.01, ***P<0.001

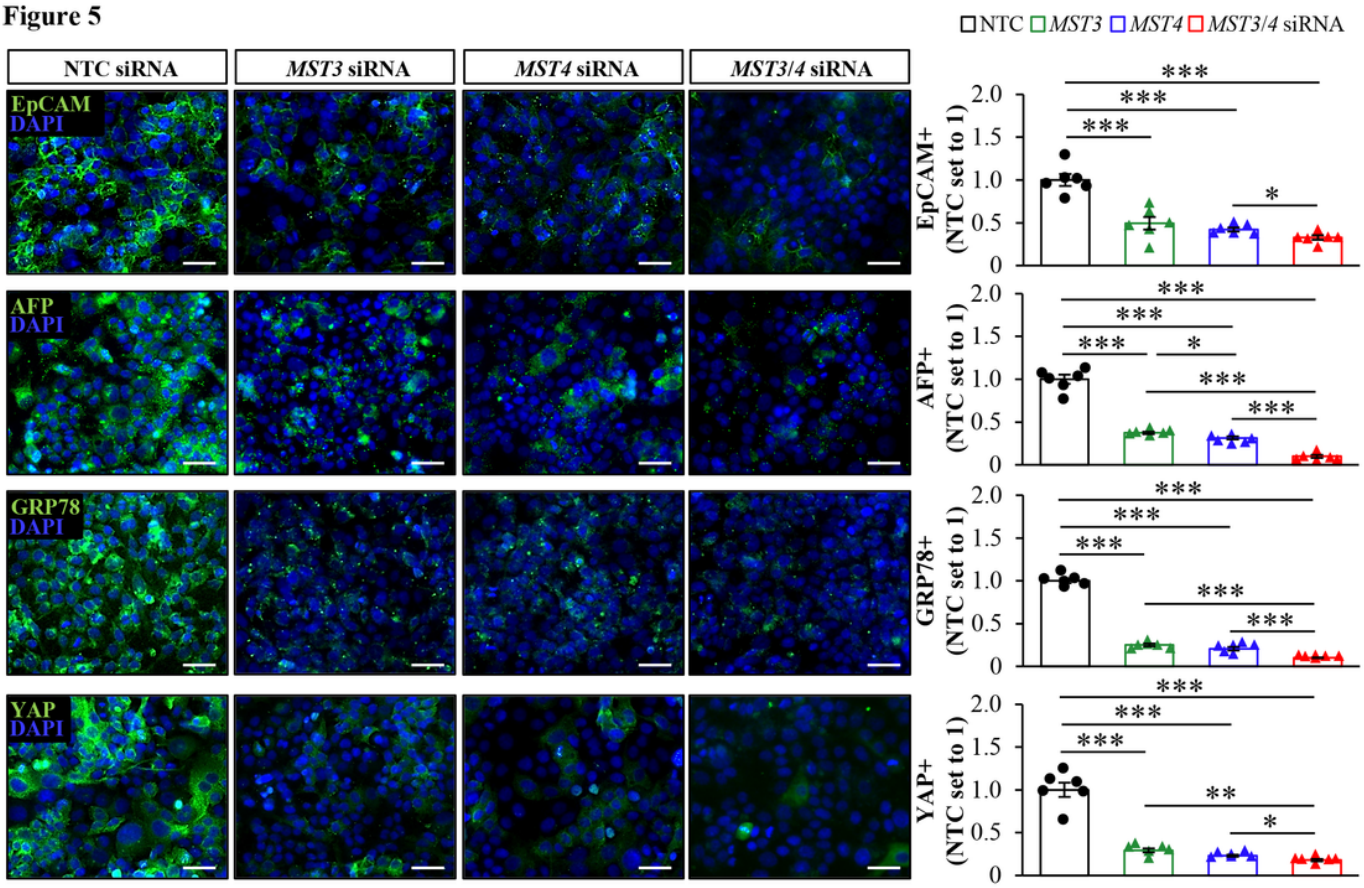

Figure 5

Knockdown of MST3 and MST4 in human HCC cells results in a lower expression of markers associated with poor prognosis of HCC. HepG2 cells were transfected with *MST3* and/or *MST4* siRNA, or NTC siRNA, and cultured with oleate supplementation. Representative images of cells processed for immunofluorescence with anti-EpCAM, anti-AFP, anti-GRP78, or anti-YAP (green) antibodies; nuclei stained with DAPI (blue). The scale bars represent 25 µm. Quantification of the staining. Data are mean ± SEM from 6 wells per group. *P<0.05, **P<0.01, ***P<0.001

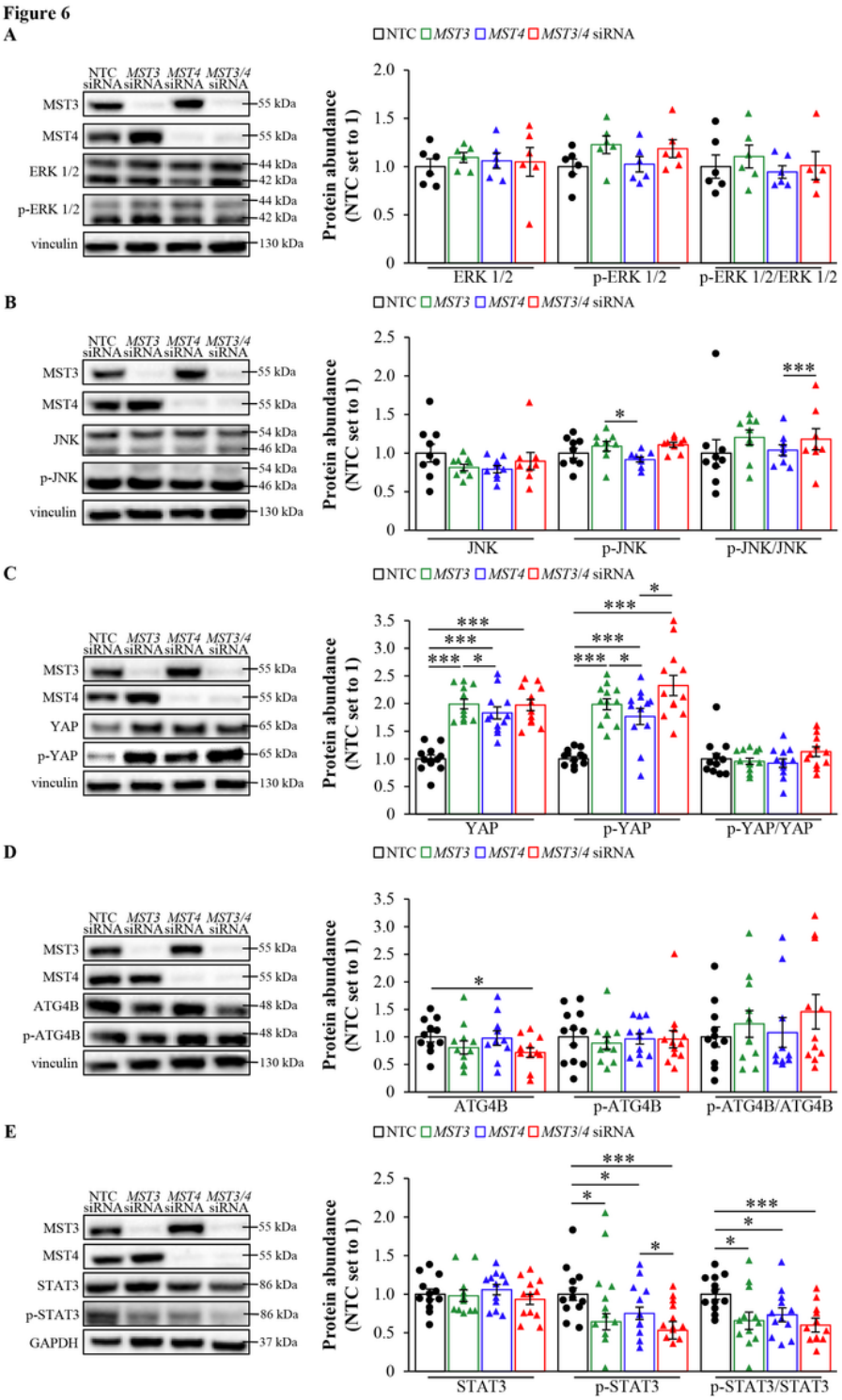

Figure 6

Silencing of MST3 and MST4 alters the pro-oncogenic pathways in human HCC cells. HepG2 cells were transfected with *MST3* and/or *MST4* siRNA, or NTC siRNA, and cultured with oleate supplementation. (*A-E*) Cell lysates analyzed by Western blot using antibodies specific for ERK1/2 or phospho-ERK1/2 (Thr^{202}/Tyr^{204}) (*A*), JNK1/2 or phospho-JNK1/2 (Thr^{183}/Tyr^{185}) (*B*), YAP or phospho-YAP (Ser^{127}) (*C*), ATG4B or phopho-ATG4B (Ser^{383}) (*D*), STAT3 or phospho-STAT3 (Thr^{705}) (*E*), MST3, or MST4. Protein

levels analyzed by densitometry; representative Western blots are shown with vinculin or GAPDH used as a loading control. Data are mean ± SEM from 5-8 (*A-B*) or 10-12 (*C-E*) wells per group. **P*<0.05, ****P*<0.001

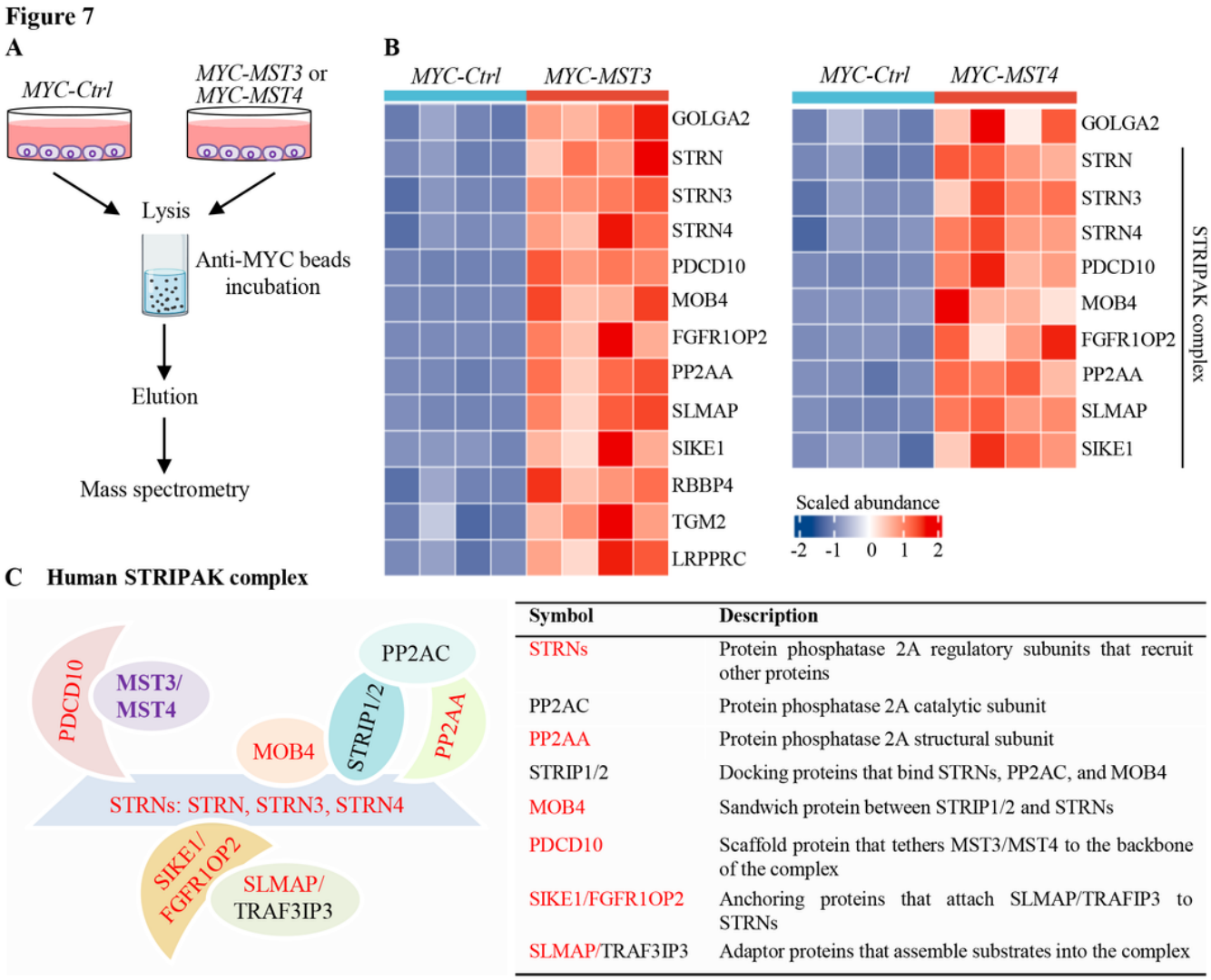

Symbol	Description
STRNs	Protein phosphatase 2A regulatory subunits that recruit other proteins
PP2AC	Protein phosphatase 2A catalytic subunit
PP2AA	Protein phosphatase 2A structural subunit
STRIP1/2	Docking proteins that bind STRNs, PP2AC, and MOB4
MOB4	Sandwich protein between STRIP1/2 and STRNs
PDCD10	Scaffold protein that tethers MST3/MST4 to the backbone of the complex
SIKE1/FGFR1OP2	Anchoring proteins that attach SLMAP/TRAFIP3 to STRNs
SLMAP/TRAF3IP3	Adaptor proteins that assemble substrates into the complex

Figure 7

MST3 and MST4 interact with GOLGA2 and the STRIPAK complex in human HCC cells. (*A*) Graphic presentation of immunoprecipitation and mass spectrometry experiments in HepG2 cells transfected with *MYC-MST3*, *MYC-MST4*, or an empty control plasmid. (*B*) Heatmaps of the scaled abundance of the identified binding partners of MST3 and MST4, see Supplementary Table S3 for details. (*C*) Schematic model of the human STRIPAK complex adapted from (77, 78). Proteins which were found to interact with MST3 and MST4 in this study are shown in red.

Figure 8

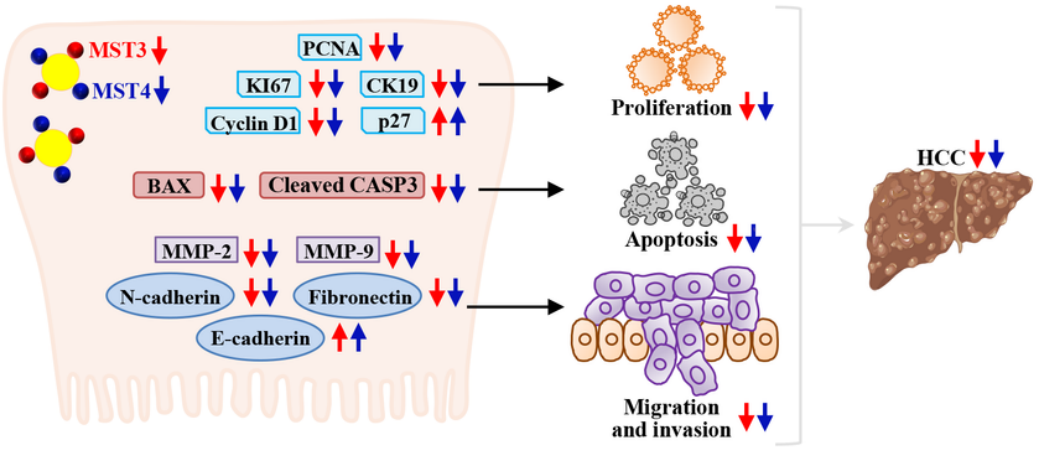

Figure 8

Silencing of MST3 and/or MST4 protects against HCC development and progression by alleviating proliferation and apoptosis and by suppressing the migration, invasion, and EMT of human HCC cells.

Supplementary Files

This is a list of supplementary files associated with this preprint. Click to download.

- Graphicalabstract230214.pdf
- SupplementaryFigureS1toS5230214.pdf
- SupplementaryTableS1230214.docx
- SupplementaryTableS2230214.docx
- SupplementaryTableS3230214.docx